Incorporation of Different Metal Ion for Tuning Color and Enhancing Antioxidant Activity of Curcumin/Palygorskite Hybrid Materials

Shue Li[1,2], Bin Mu[1]*, Penji Yan[3], Yuru Kang[1], Qin Wang[1] and Aiqin Wang[1]*

[1]Key Laboratory of Clay Mineral Applied Research of Gansu Province, Center of Eco-Material and Green Chemistry, Lanzhou Institute of Chemical Physics, Chinese Academy of Sciences, Lanzhou, China, [2]Center of Materials Science and Optoelectronics Engineering, University of Chinese Academy of Sciences, Beijing, China, [3]Key Laboratory of Hexi Corridor Resources Utilization of Gansu Universities, College of Chemistry and Chemical Engineering, Hexi University, Zhangye, China

Curcumin is one of the dietary dyes extracted from turmeric and used for prevention and treatment of various illnesses. However, the low bioavailability and poor stability of curcumin limits its relevant applications. Therefore, different metal ions including Cu^{2+}, Zn^{2+}, Mg^{2+}, Al^{3+}, or Fe^{3+} were incorporated to tune the color, enhance the environmental stability and antioxidant activity of curcumin in the presence of palygorskite in this study. The as-prepared samples were studied using X-ray diffraction, Fourier transform infrared spectroscopy, X-ray photoelectron spectroscopy, Zeta potential, and transmission electron microscopy. In addition, the density functional theory calculation was also performed to explore the possible interaction among metal ions, curcumin and palygorskite. It was found that the color changing and stability enhancing were ascribed to the curcumin-metal ions coordination as well as chemical interactions between curcumin-metal complex and palygorskite. Moreover, the as-prepared composites showed more excellent color, thermal stability, antioxidant activity, and fluorescence properties than that of the curcumin/palygorskite composites due to the presence of metal ions. The finding of this investigation may contribute to developing the multifunctional composites with different colors and good antioxidant activity for relevant applications based on curcumin and palygorskite.

Keywords: curcumin, palygorskite, metal ions, color tuning, antioxidant activity, stability

INTRODUCTION

It has long been known that many over-the-counter natural products can be used to treat and prevent a variety of chronic diseases. Among them, some of dietary polyphenols including curcumin (Cur), anthocyanin and resveratrol have attracted considerable attention because of their useful therapeutics (Jin 2018). In particular, Cur, a kind of naturally occurring yellow polyphenols, was extracted from the rhizomes of Curcuma longa or turmeric and used for centuries in varieties pharmaceutical applications towards various diseases due to the general biological and pharmaceutical activity (Barik et al., 2007; Kumar et al., 2020b). As a result, the green and low-toxic index natural product was widely used as traditional medicine, food coloring and flavoring agent, and a cosmetic agent for skin care for its antioxidant activities, anti-thrombotic and other health benefits (Pourreza et al., 2018; Lin et al., 2020). From the structure of Cur molecule (1,7-bis-(4-hydroxy-3-methoxyphenyl)-1,6-heptadiene-3,5-dione), it has a lot of available metal binding sites. Cur chelate with metal ions through the central

GRAPHICAL ABSTRACT |
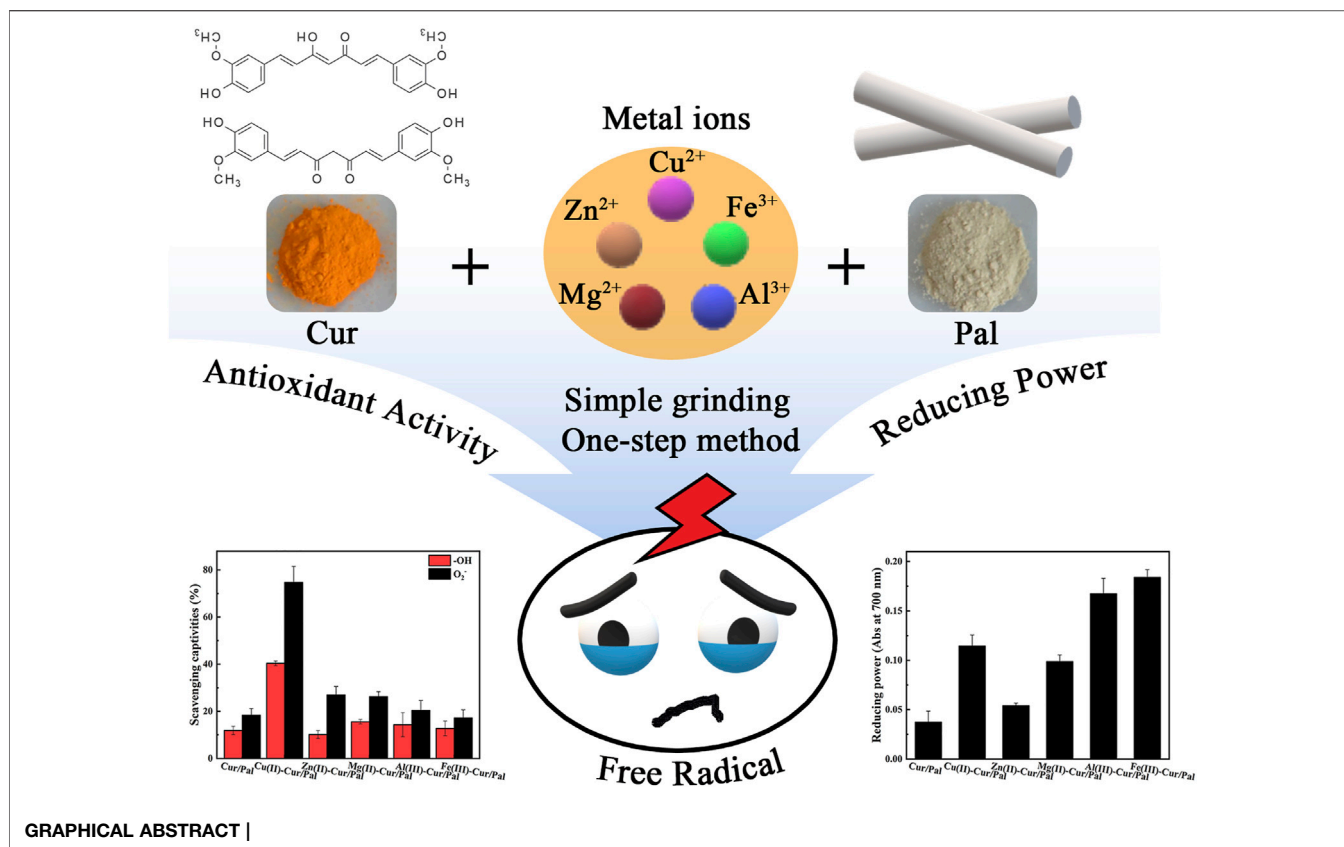
β-diketone functionality of molecular structure to form the more stable complexes and scavenge the reactive oxygen species (Zhao et al., 2010). Beyond that, one hydroxyl group attached on each of the two benzene rings plays a major role in antioxidant activity of Cur (Priyadarsini et al., 2003). At present, there are many reports that the metal ions complexes of Cur are very useful for curing various diseases due to their higher anti-oxygen activity, better antimicrobial property and aqueous stability, as well as antitumor and anticancer effect (Barik et al., 2007; Refat, 2013; Zhang et al., 2016; Mary et al., 2018; Wang et al., 2020).

However, the poor stability of Cur reduced the acceptance of consumers, which restricted the application of Cur as a functional ingredient in food (Hu et al., 2020). As a result, a number of strategies including encapsulation into liposomes (Cheng et al., 2017), the loading of nanoparticles (Arab et al., 2021; Yuan et al., 2021), chemical modifications by polymer conjugates (Li et al., 2020b; Chen et al., 2020), plasmonic nanogel (Howaili et al., 2020), and complexation with proteins (Mohammadian et al., 2019; Hu et al., 2020) have been applied to stabilize Cur and expand its relevant applications. But beyond all that, clay minerals deserve more attention because of their safety, low-cost and excellent performances. To the authors' knowledge, there are still very few studies on Cur and clay minerals in the last few years. Previously, Cur-Au hybrid nanoparticles loaded halloysite nanotubes were developed by *in-situ* preparation method and then coated with bio-adhesive chitosan, making them exhibit the

NIR responsive and pH-responsive properties (Rao et al., 2018). Some research had focused on the development of montmorillonite systems, with or without modification, as a kind of Cur carrier in order to achieve Cur stabilization and improve its availability (Madusanka et al., 2015; Gonalves et al., 2017).

It is well-known that palygorskite (Pal), a nanorod-like hydrated magnesium-rich aluminosilicate clay mineral, is renowned for its ability to stable natural indigo dye (Xu et al., 2017). What's more, Pal possessed regular nanochannel structure has unique crystal morphology, large active surface groups and specific surface area, resulting in the good adsorption efficiency. As early as 1966, van Olphen confirmed, as Dogenech-Carbo et al. later demonstrated, that Pal was more beneficial than other clay minerals in stabilizing the natural indigo molecules (Van Olphen, 1966; Domenech-Carbo et al., 2013). To date, in order to stabilize natural pigments, such as betanin, flavylium cations and anthocyanin, and expand their application fields, Pal-based hybrid pigments have been developed due to the excellent performances, such as superior stability, fluorescence and acid/base reversible allochroic behavior (Silva et al., 2018; Li et al., 2019a; Li et al., 2020a). In this context, Pal is an attractive supporting matrix that can be employed as an inorganic carrier to stabilize Cur molecules.

In this paper, Cur/Pal and a series of metal ion-Cur/Pal hybrid materials with different yellow hues were prepared. The main objective of this research is to explore the effect of the different metal ion on the color, thermal stability, antioxidant activity, and

fluorescence properties of Cur/Pal. Based on their excellent properties, the synthesized the multifunctional composites with different colors and good antioxidant activity had the good application prospects.

EXPERIMENTAL

Materials and Methods

Palygorskite (Pal) was supplied by Guanshan Mine, Anhui Province, China. Curcumin (Cur) was purchased from the Afaisha (China) Chemical Co., Ltd., Shanghai, China. Other chemicals were of analytical grade from commercial sources.

Synthesis of Metal Ions-Cur/Pal Hybrid Materials

Metal ions-Cur/Pal hybrid materials were synthesized employing the simple one-step method by mixing Cur with copper acetate monohydrate, zinc acetate dihydrate, magnesium acetate tetrahydrate, aluminium chloride hexahydrate, and ferric chloride at a molar ratio of 1:2, 1:1, 1:1, 1:2, and 1:2, respectively. Briefly, 0.1359 g of copper acetate monohydrate, 0.2989 g of zinc acetate dihydrate, 0.2908 g of magnesium acetate tetrahydrate, 0.1637 g of aluminium chloride hexahydrate or 0.1834 g of ferric chloride was added into 0.5 g of Cur dissolved in 2 ml ethanol with 4 ml distilled water with a pH of 4.0 adjusted by HCl aqueous solutions (except for copper acetate monohydrate), respectively. And then, 1 g of Pal was added to the above mixture and ground under dark conditions for 30 min to obtain a series of samples. In order to remove the excess Cur and metal ions, the mixture was washed with 100 ml deionized water and anhydrous ethanol for three times, respectively, after vacuum drying at 60°C for 2 h. It was worth noting that the samples of each washing were centrifuged at 4,000 rpm for 10 min to achieve solid-liquid separation. Finally, the final products were obtained after being placed overnight in a vacuum drying oven at 60°C. The samples were labeled as Cu(II)-Cur/Pal, Zn(II)-Cur/Pal, Mg(II)-Cur/Pal, Al(III)-Cur/Pal, and Fe(III)-Cur/Pal, respectively. The sample without metal salts involved in the preparation process was labeled as Cur/Pal.

Characterization

The Fourier transform infrared (FTIR) spectra, transmitting electron microscopy (TEM), powder X-ray diffraction (XRD) analysis, Zeta potentials, Field emission transmission electron microscopy (TEM), and X-ray photoelectron spectroscopy (XPS) of the samples were obtained according to our previously reported methods (Li et al., 2020a). The elemental analysis of all samples was determined by Elementar analyzers varioEL cube (Elementar Analysen systeme GmbH, Germany). Thermogravimetric analysis (TGA) was conducted on a STA8000 simultaneous thermal analyzer (PerkinElmer, United States) at a heating rate of 10°C min^{-1} under a N$_2$ atmosphere, and the initial mass of all samples was about 0.005 g. The color parameters of all as-prepared samples were evaluated using a Color-Eye automatic differential colorimeter (X-Rite, Ci 7800, Pantone Inc, United States) on the basis of the CIE 1976 $L^*a^*b^*$ colorimetric method, in which L^* is the color lightness (from 0 (black) to 100 (white)), negative/positive a^* is the red/green axis, and negative/positive b^* is the yellow/blue axis. Chromaticity (C^*) and hue angle ($h°$) are calculated by **Eqs 1**, **2**:

$$C^* = \left\{ (a^*)^2 + (b^*)^2 \right\}^{1/2} \qquad (1)$$

$$h° = \arctan (b^*/a^*) \qquad (2)$$

The color difference in the CIE $L^*a^*b^*$ space was evaluated using ΔE^* calculated according to **Eq.3**:

$$\Delta E^* = \left\{ (\Delta L^*)^2 + (\Delta a^*)^2 + (\Delta b^*)^2 \right\}^{1/2} \qquad (3)$$

Furthermore, the reflectance and corresponding UV-vis spectra were obtained from X-Rite, Ci 7800.

Computational Details and Models

In order to cognize the loading mechanism, the DFT and TD-DFT calculations were performed based on the Gaussian 09 (Frisch et al., 2009) program and carried out using M062X (D3) (Zhao and Truhlar 2008; Grimme et al., 2010) function combined with the 6-31G(d) basis set for Si, O, Mg, Al, and H. The Stuttgart/Dresden effective core pseudopotentials (SDD) basis set was used for Cu, Zn, and Fe. Based upon the optimized structures, the UV-visible spectra properties of the Cur molecules and metal-Cur complexes, metal-Cur-Pal complexes were calculated adopting the time-dependent DFT (TD-DFT) method with the B3LYP(D3BJ)/6-31G(d) (Becke 1993; Grimme 2006; Schwabe and Grimme 2007) basis set in dimethyl sulfoxide (DMSO) media with the Solvation Model Density (SMD) (Marenich et al., 2009) implicit solvation model. The electrostatic potential (ESP) was generated on vdW surface depended on Multiwfn 3.8 (Lu and Chen 2012) and was visually presented using Visual Molecular Dynamics (VMD) software (Humphrey et al., 1996). We have used Gauss View program (Dennington et al., 2009) to generate ball and stick geometries of optimized structures.

Thermal Stability of Metal Ions-Cur/Pal Hybrid Materials

The thermal stabilities based on colour change of Cur/Pal and series of metal ions-Cur/Pal hybrid materials were tested by placing the samples in an oven at 120, 150, 180, and 210°C for 30 min, respectively.

Fluorescence Properties of Metal Ions-Cur/Pal Hybrid Materials

The fluorescence spectra of DMSO suspension of Cur, Cur/Pal and series of metal ions-Cur/Pal hybrid materials was conducted using a HORIBA Fluorolog-3 spectrofluorometer (HORIBA Instruments Inc, United States), and recorded by monitoring fluorescence excitation at 435 nm.
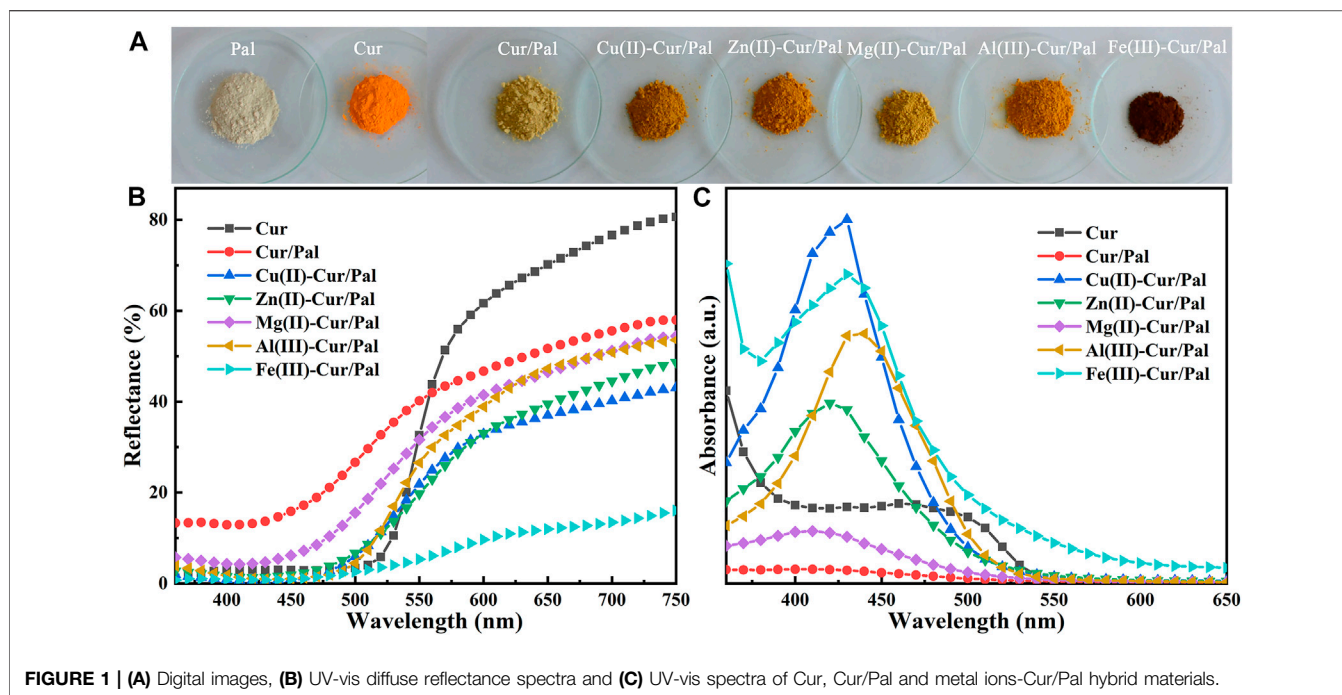
FIGURE 1 | (A) Digital images, **(B)** UV-vis diffuse reflectance spectra and **(C)** UV-vis spectra of Cur, Cur/Pal and metal ions-Cur/Pal hybrid materials.

Free Radical Scavenging Experiments

The superoxide free radical scavenging ability of the as-prepared samples was determined by the pyrogallol autoxidation method described previously with slight modifications (Li, 2012). 200 μL DMSO containing sample was mixed with 2,700 μL of Tris-HCl buffer (0.05 M, pH 8.2) and then heated in a water bath at 37°C for 4min after shaken vigorously for several seconds. Subsequently, 100 μL of pyrogallol solution (60 mM in 1 mM HCl, 37°C) was added to the above mixture, immediately vigorously shaken, and then send to measure its absorbance at 325 nm every 30 s for 5 min using UV-vis spectrometer (UV-1900, Shimadzu, Japan). The superoxide free radical scavenging ability was calculated using the following **Eq. 4**:

$$\text{Scavenging ability}\,(\%) = \{(\Delta A_0 - \Delta A_S + \Delta A_{S0})/\Delta A_0\} \times 100\% \tag{4}$$

where, ΔA_0 is the increase of absorbance at 325 nm in 5 min of the mixture without the sample and ΔA_S is that of the mixture with the sample, respectively. ΔA_{S0} is the absorbance at 325 nm of sample without pyrogallol solution. The assay was repeated for three times.

The ability of scavenging the hydroxyl radicals for all samples were tested the absorbance at 510 nm, according to the previous report (Wei et al., 2021). At first, 1.8 M ferrous sulfate solution, 1.8 M hydrogen peroxide solution and 1.8 M salicylic acid-ethanol solution were prepared in advance. After that, solution A_0 was obtained by adding salicylic acid-ethanol solution (2 ml), ferrous sulfate solution (2 ml) and hydrogen peroxide solution (2 ml) into DMSO (2 ml). In the case of the sample, 2 ml of salicylic acid-ethanol solution, ferrous sulfate solution, hydrogen peroxide solution and sample solution were mixed to obtain

solution A_S. 2 ml of salicylic acid-ethanol solution, ferrous sulfate solution and sample solution was mixed to prepare solution A_{S0}. Finally, the absorbance of three solutions at 510 nm was determined after being incubated at 37°C for 30 min. The hydroxyl free radical scavenging rate can be calculatedby following formula:

$$\text{Scavenging ability}\,(\%) = \{(A_0 - A_S + A_{S0})/A_0\} \times 100\% \tag{5}$$

Reducing Power

Reducing power of the as-prepared samples was determined according to the previous method (Gulcin et al., 2004; Hu et al., 2020). Each sample DMSO solution (1 ml) was blended with PBS (2.5 ml, 0.2 M, pH 6.6) and $K_3Fe(CN)_6$ solution (2.5 ml,1%, w/v), and then incubated in water bath at 50°C for 20 min. After that, trichloroacid (2.5 ml,10%, w/v) was added and centrifuged at 4,000 rpm for 10 min. Supernatant (2.5 ml) was blended with 2.5 ml of deionized water and 0.5 ml $FeCl_3$ solution (0.1%,w/v), and stored at room temperature for 10 min. The absorbance at 700 nm of each sample was then documented. It should be noted that higher absorbance of the reaction mixture demonstrated greater reductive potential.

RESULTS AND DISCUSSION

Synthesis and Characterization of Metal Ions-Cur/Pal

Digital images, UV-vis diffuse reflectance spectra and UV-vis spectra of Cur, Cur/Pal and metal ions-Cur/Pal hybrid materials
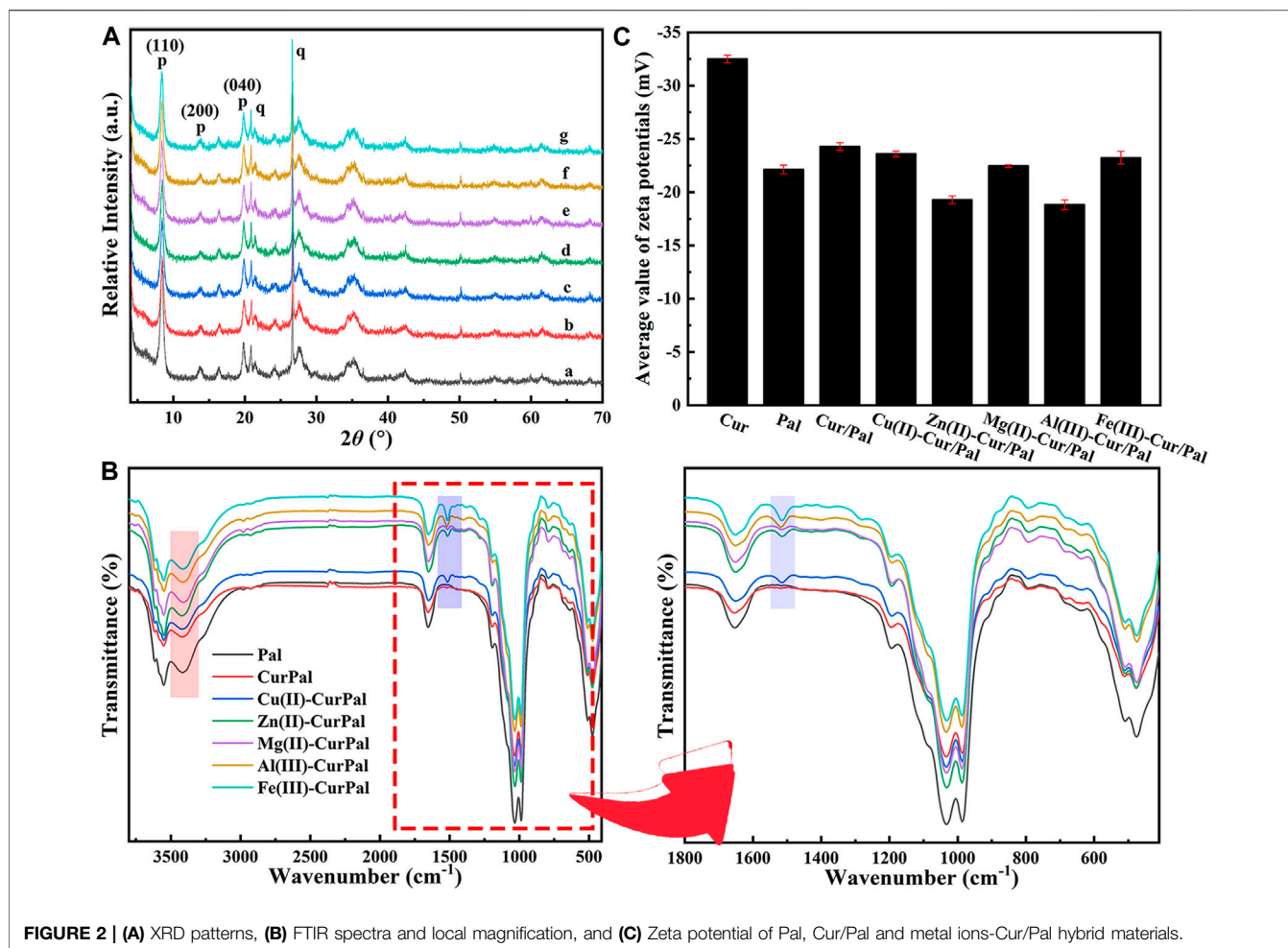
FIGURE 2 | (A) XRD patterns, (B) FTIR spectra and local magnification, and (C) Zeta potential of Pal, Cur/Pal and metal ions-Cur/Pal hybrid materials.

are shown in **Figure 1**. Effects of Cu^{2+}, Zn^{2+}, Mg^{2+}, Al^{3+}, and Fe^{3+} on the color of Cur/Pal hybrid materials were investigated. It was obviously observed that Pal and Cur are off white and saffron yellow in color, respectively. Compared with pure Cur, the yellow color of the Cur/Pal hybrid materials became lighter obviously after introduction of Pal. However, the tone of the hybrid materials was significantly changed by adding metal ions (**Figure 1A**; **Supplementary Figure S1**). As shown in **Supplementary Table S1**, a^* and b^* values of Cur/Pal with different metal ions (except for Fe^{3+}) increased obviously, which was suggested that the redness and yellowness of metal ions-Cur/Pal were enhanced compared with that of Cur/Pal. Among them, Al(III)-Cur/Pal presented the reddest and yellowest values, suggesting that Al^{3+} was more conducive to the color enhancement of Cur/Pal. In the same case, L^* values representing brightness was reduced and the color of the obtained samples became darker than Cur/Pal. The above results indicated that the participation of metal ions might improve the loading capacity of Pal to Cur (Gutiérrez et al., 2017). In addition, the increase in the C^* values and decrease in the h° values were also observed when Cu^{2+}, Zn^{2+}, Mg^{2+}, Al^{3+}, and Fe^{3+} was incorporated into Cur molecule and Pal, respectively. It indicated that the metal ions-Cur/Pal samples presented a

more vivid color in yellow or orange zone (Li et al., 2019b). In addition, the reflectance spectra of hybrid materials prepared with different metal ions, Cur, and Pal were evaluated (**Figure 1B**), and the strong absorption mainly of all samples happened in wavelength of 400–550 nm of the visible region, including the blue and green light region (Wang et al., 2018). Hence, these samples presented their complementary color of yellow or orange-yellow. Moreover, a blue shift on the optical absorption bands was also observed for all metal ions-Cur/Pal hybrid materials compared with that of the pure Cur (**Figures 1B,C**).

Figure 2A is the XRD patterns of Pal, Cur/Pal and the corresponding metal ions-Cur/Pal hybrid materials. The characteristic diffraction peaks of Pal crystal have been determined from the diffractograms, which was consistent with those reported in the literatures (Li et al., 2019a; Lu et al., 2019). In addition, small amounts of quartz in Pal had been found. However, no characteristic peaks of Cur crystal phases were observed for the Cur/Pal and metal ions-Cur/Pal hybrid materials due to the transformation from crystalline to the X-ray amorphous nature of Cur (Kumar et al., 2020a). FTIR spectra of as-prepared Cur/Pal and metal ions-Cur/Pal hybrid materials were shown in **Figure 2B**. In the spectrum of Pal, the
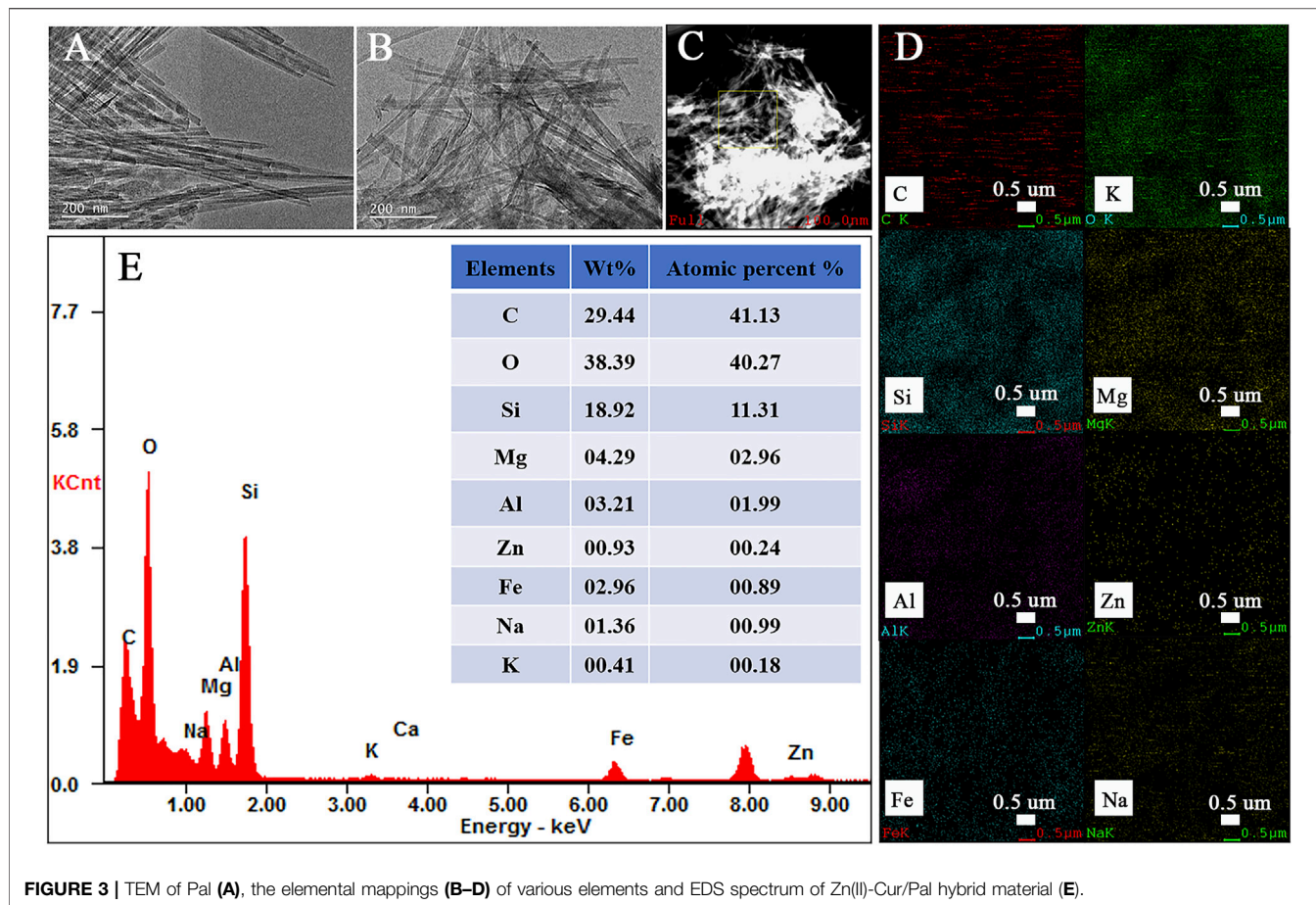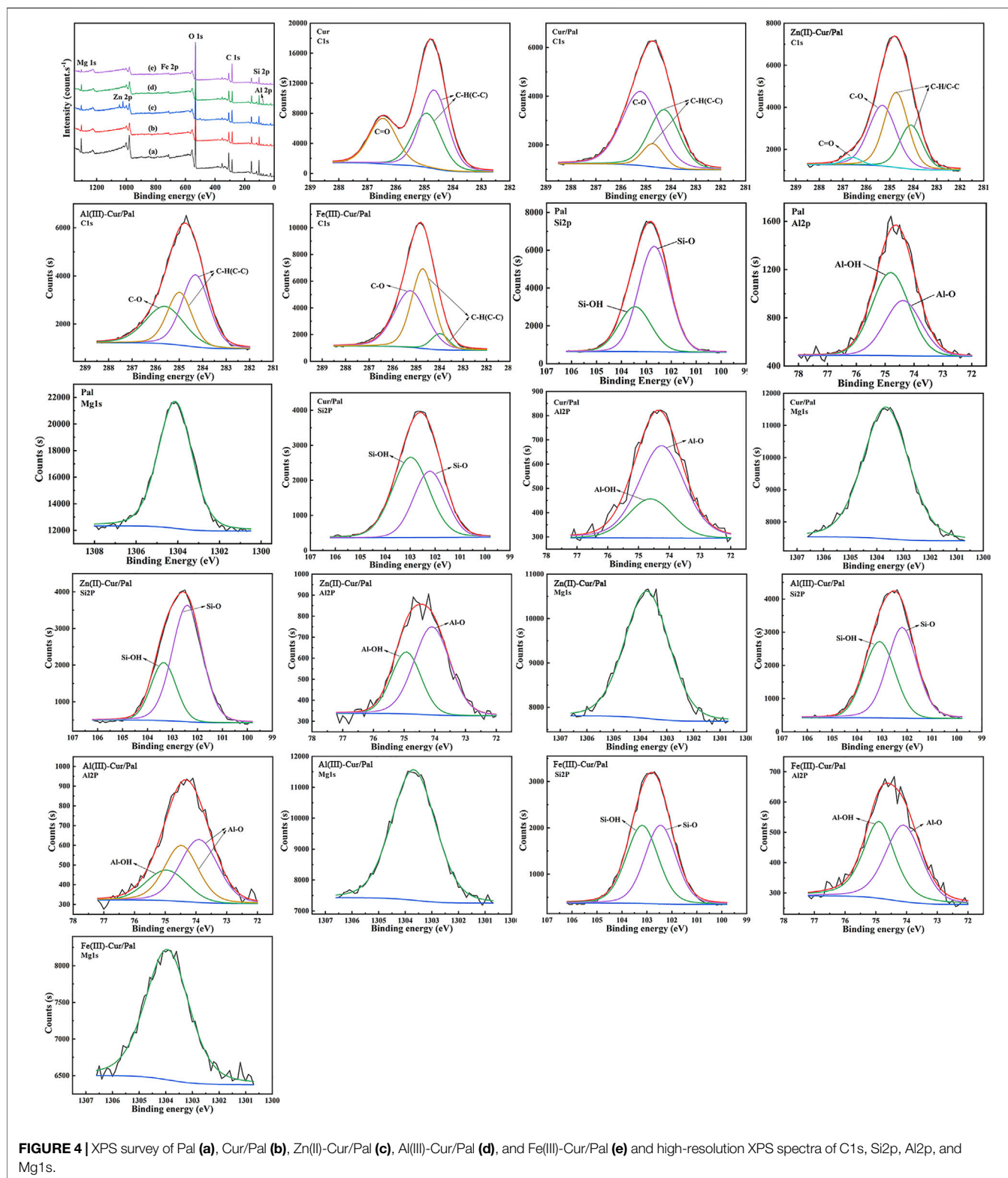
FIGURE 3 | TEM of Pal **(A)**, the elemental mappings **(B–D)** of various elements and EDS spectrum of Zn(II)-Cur/Pal hybrid material **(E)**.

absorption peak observed in the wavelength between $3,430 \, cm^{-1}$ and $3,400 \, cm^{-1}$ was due to the hydroxyl stretching vibration of coordinated water located at terminal positions of the octahedral sheets, physical-adsorbed water on Pal surface and zeolitic H_2O inside Pal channels (Zhang et al., 2015a; Carazo et al., 2018; Li et al., 2019a). The OH bending vibration of the above water molecules appeared at ca. $1650 \, cm^{-1}$ (Miao et al., 2020). In detail, the hydroxyl stretching and bending vibrations were shifted from the values of 3,416 and $1653 \, cm^{-1}$ for Pal to 3,409 and $1650 \, cm^{-1}$ for Cur/Pal, 3,419 and $1650 \, cm^{-1}$ for Cu(II)-Cur/Pal, 3,422 and $1650 \, cm^{-1}$ for Zn(II)-Cur/Pal, 3,410 and $1651 \, cm^{-1}$ for Mg(II)-Cur/Pal, 3,414 and $1650 \, cm^{-1}$ for Al(III)-Cur/Pal, 3,413 and $1651 \, cm^{-1}$ for Fe(III)-Cur/Pal, respectively. Significantly, both bands were shifted in the Cur/Pal and metal ions-Cur/Pal hybrid materials because of the H-bonding of carbonyl group of Cur with complexion water existed in the channels of Pal. In addition to the characteristic peaks of Pal, the new characteristic band associated with C=C stretching vibration of benzene rings of Cur was also observed at $1515 \, cm^{-1}$ in the spectrum of metal ions-Cur/Pal hybrid materials (Madusanka et al., 2015; Zhou and Tang 2016). However, the bands of Cur/Pal were identical to that of Pal except in their intensities because of the low concentration of Cur in Pal, which resulted in no clearly visible bands being observed (Ma et al., 2017).

Cur had a Zeta potential value of −32.50 mV, which was due to the negative charged phenol groups (**Figure 2C**) (Liao et al., 2018). The Zeta potential was −24.30 mV, −23.6 mV, −19.3 mV, −22.47 mV, −18.83 mV, and −23.23 mV for Cur/Pal, Cu(II)-Cur/Pal, Zn(II)-Cur/Pal, Mg(II)-Cur/Pal, Al(III)-Cur/Pal, and Fe(III)-Cur/Pal, respectively, after incorporation of Pal and different metal ions. Compared with Pal (−22.13 mV), the Zeta potential values of as-prepared samples remained negative. Remarkably, the slight increase in the Zeta potential values of Zn(II)-Cur/Pal and Al(III)-Cur/Pal indicated the formation of electrostatic interaction. In the cases of Cur/Pal, Cu(II)-Cur/Pal, Mg(II)-Cur/Pal, and Fe(III)-Cur/Pal, hydrogen bonding interaction between compositions should predominate in such systems.
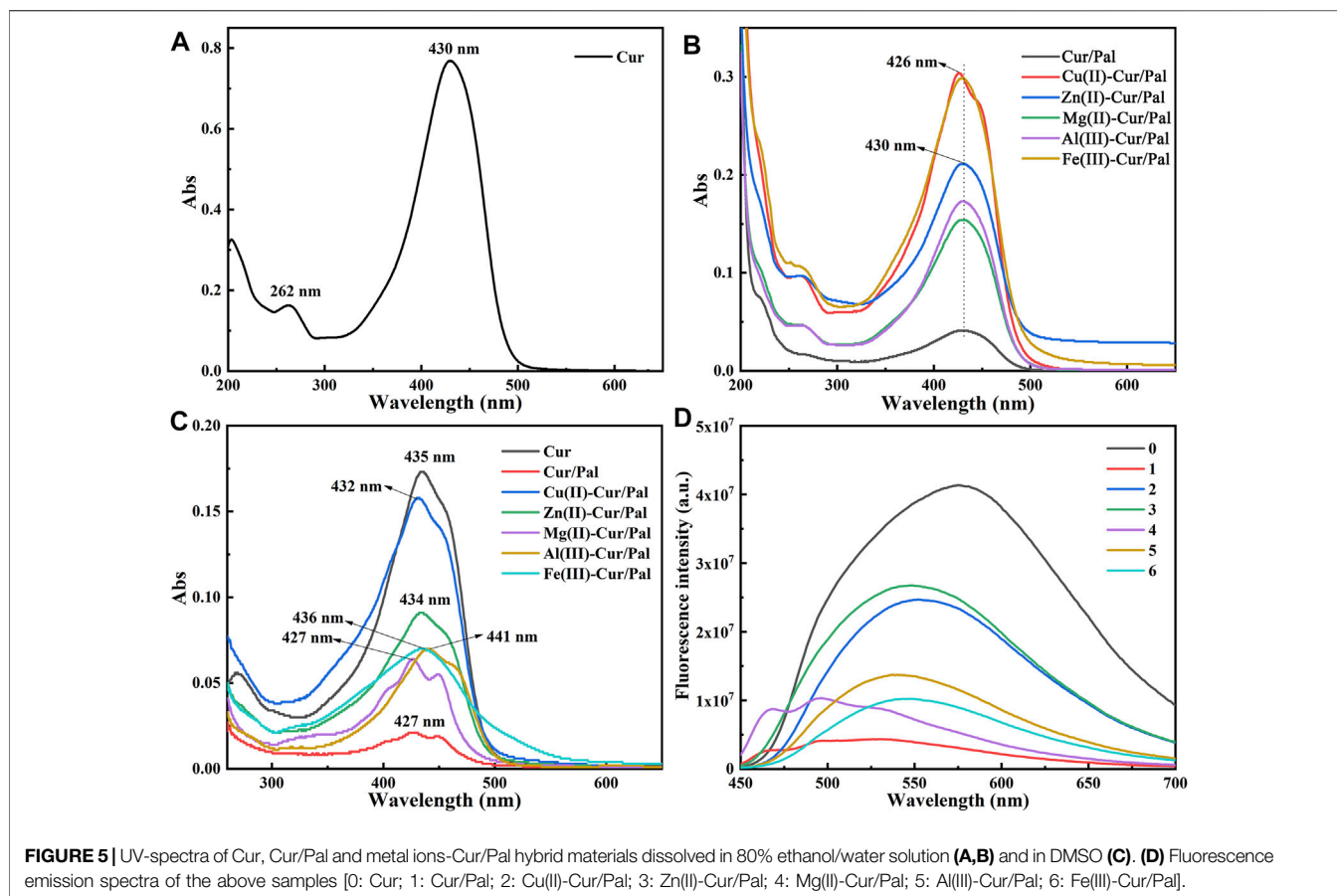
The major elements within the Zn(II)-Cur/Pal hybrid material are qualitatively detected by EDS elemental analysis (**Figure 3**). As shown in **Figures 3A,B**, it was worth mentioning that the representative rod-like morphology of Pal was retained and the crystal bundles in the sample were better disaggregated by grinding. The elemental mappings and EDS spectrum are presented in **Figures 3D,E**, which confirmed that the distribution of C, O, Si, Mg, Al, Zn, Fe, Na, and K is highly uniform in Zn(II)-Cur/Pal samples, indicating that Zn(II)-Cur complex was formed on Pal matrix. In addition, the elemental analysis (C%) of the Cur/Pal and metal ions-Cur/Pal hybrid

FIGURE 4 | XPS survey of Pal **(a)**, Cur/Pal **(b)**, Zn(II)-Cur/Pal **(c)**, Al(III)-Cur/Pal **(d)**, and Fe(III)-Cur/Pal **(e)** and high-resolution XPS spectra of C1s, Si2p, Al2p, and Mg1s.

materials was listed in **Supplementary Table S2**, in which C% of Cur/Pal, Cu(II)-Cur/Pal, Zn(II)-Cur/Pal, Mg(II)-Cur/Pal, Al(III)-Cur/Pal, and Fe(III)-Cur/Pal hybrid materials was 1.26, 2.41, 2.07, 1.61, 2.33, 3.51%, respectively. It indicated that the

content of Cur in as-prepared metal ions-Cur/Pal samples was higher than that of Cur/Pal.

XPS analysis elucidate the chemical state of the surface C1s, Si2p, Al2p, Mg1s, Zn2p, Fe2p element content in the surface

FIGURE 5 | UV-spectra of Cur, Cur/Pal and metal ions-Cur/Pal hybrid materials dissolved in 80% ethanol/water solution **(A,B)** and in DMSO **(C)**. **(D)** Fluorescence emission spectra of the above samples [0: Cur; 1: Cur/Pal; 2: Cu(II)-Cur/Pal; 3: Zn(II)-Cur/Pal; 4: Mg(II)-Cur/Pal; 5: Al(III)-Cur/Pal; 6: Fe(III)-Cur/Pal].

analyses of the Cur, Pal, Cur/Pal, Zn(II)-Cur/Pal, Al(III)-Cur/Pal, and Fe(III)-Cur/Pal hybrid materials. The wide range spectra of the Pal, Cur/Pal, Zn(II)-Cur/Pal, Al(III)-Cur/Pal, and Fe(III)-Cur/Pal are presented in **Figure 4**. As expected, the pristine Pal surface was characterized by the existence of Si, Al, Mg, Fe, and O, as well as some adventitious C (**Supplementary Table S3**). After treatment, the O1s, Si2p, Al2p, and Mg1s peaks were weaker compared with the spectrum of Pal, whereas the C1s peak was much stronger in as-prepared samples. The high C content in the Cur/Pal, Zn(II)-Cur/Pal, Al(III)-Cur/Pal, and Fe(III)-Cur/Pal hybrid materials was owing to the presence of Cur. In addition, Zn(II)-Cur/Pal exhibited one new low intensity peaks at 1022 eV compared with Cur/Pal, which was in keeping with Zn2p valence band region. Moreover, there are differences in C1s spectra in Cur, Pal and as-prepared samples as shown in **Figure 4**, **Supplementary Figure S2** and **Supplementary Table S4**. In the case of Cur, the Cls region could be fitted into three peaks located at around 284.66, 284.91 and 286.45 eV, which were ascribed to C-C and C-H linkages, C=O bonds, respectively (Mandal et al., 2017; Moradi et al., 2020). Compared with Cur and Pal, the new peak of C1s at a binding energy of 285.22 eV related to the C-O bond became remarkably visible while the peak corresponding to C=O bonds gradually disappeared in the XPS spectra of as-prepared samples. What's more, the Si2p, Al2p, and Mg1s peaks of samples slightly shift to lower binding energy than that of Pal with an decrease in the intensity. The above results

of XPS also proved the present of Cur on the surface of Pal by complexation with metal ions.

The UV-Vis absorption spectra of Cur, Cur/Pal and metal ions-Cur/Pal hybrid materials in 80% water-ethanol are depicted in **Figures 5A,B**. The spectrum of Cur exhibited a weak absorption in the UV region attributing to the phenolicmoiety and the absorption maximum at 430 nm in the visible region due to the keto-enol moietyin a polar protic solvent (Beneduci et al., 2019). The addition of the metal cations of Zn^{2+}, Mg^{2+}, Al^{3+}, or Fe^{3+} into Cur and Pal resulted in the marked difference in their intensity, though the peaks showed no obvious shift compared with that of Cur. Notably, the peak wavelength of Cu(II)-Cur/Pal was around 426 nm and had an evident shoulder at higher wavelength with respect to Cur, which was consistent with previous reports (Picciano and Vaden, 2013). As depicted in **Figure 5C**, their spectra exhibited absorption maxima bands at 435 nm for Cur, at 427 nm for Cur/Pal, at 432 nm for Cu(II)-Cur/Pal, at 434 nm for Zn(II)-Cur/Pal, at 427 nm for Mg(II)-Cur/Pal, at 441 nm for Al(III)-Cur/Pal, at 436 nm for Fe(III)-Cur/Pal, respectively. The bands existed at 400–470 nm region could be correspond to an n→π* transitions type (Goswami et al., 2013; Refat 2013). The slight shift could be detected on the Cur/Pal and metal ions-Cur/Pal hybrid materials, indicating that the carbonyl group of Cur was involved in the reaction (Song et al., 2009; Refat 2013). It was vital that the spectra of Cur/Pal was similar to that of Mg(II)-Cur/Pal except for strength, suggesting that Cur might

FIGURE 6 | TGA curves of **(A)** Pal, Cur (the inset), **(B)** Cur/Pal and metal ions-Cur/Pal hybrid materials.
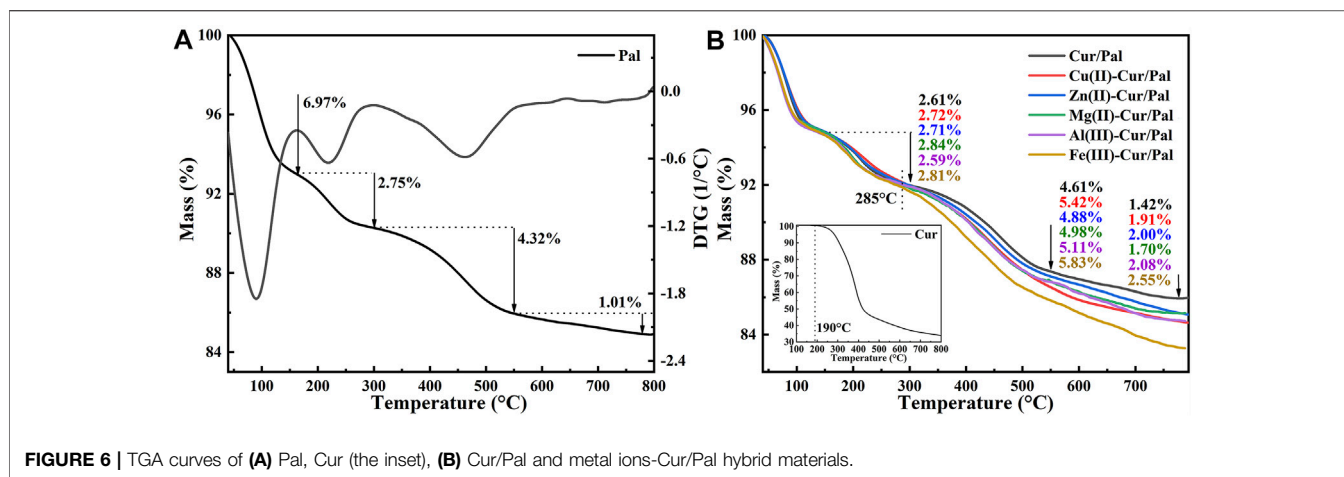
have formed a complex with OH_2, which was coordinated with Mg^{2+} at the edges of the octahedral layers of Pal.

The fluorescence emission spectra of the above-mentioned samples are presented in **Figure 5D**. In the case of Cur, the peak at ~575 nm was due to fluorescence emission. Upon the addition of various metal ions, it was interesting to note that the peak of the samples showed obvious blue shift compared with that of Cur. However, the fluorescence emission spectra of Cur/Pal and Mg(II)-Cur/Pal were similar (**Figure 5D**), that is, the shoulder appeared in the lower wavelength except for the blue shift. Therefore, it could be considered that the hypochromatic shifted emission of Cur/Pal and metal ions-Cur/Pal hybrid materials produced excitation in Cur monomers (Bhopate et al., 2015). What's more, although internal quenching of Cur would occur in the presence of metal due to complexation, the fluorescence intensity of metal ions-Cur/Pal was still obviously enhanced compared with Cur/Pal because of the higher loading of Cur. Among them, the strongest fluorescence in Zn(II)-Cur/Pal sample were observed, followed by Cu(II)-Cur/Pal, Al(III)-Cur/Pal, Mg(II)-Cur/Pal, and Fe(III)-Cur/Pal in sequence.

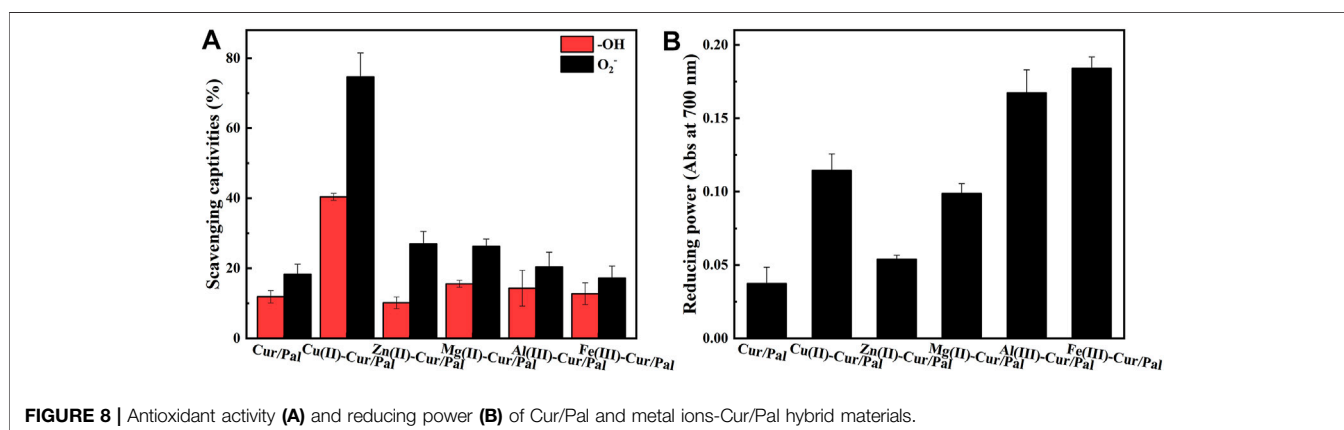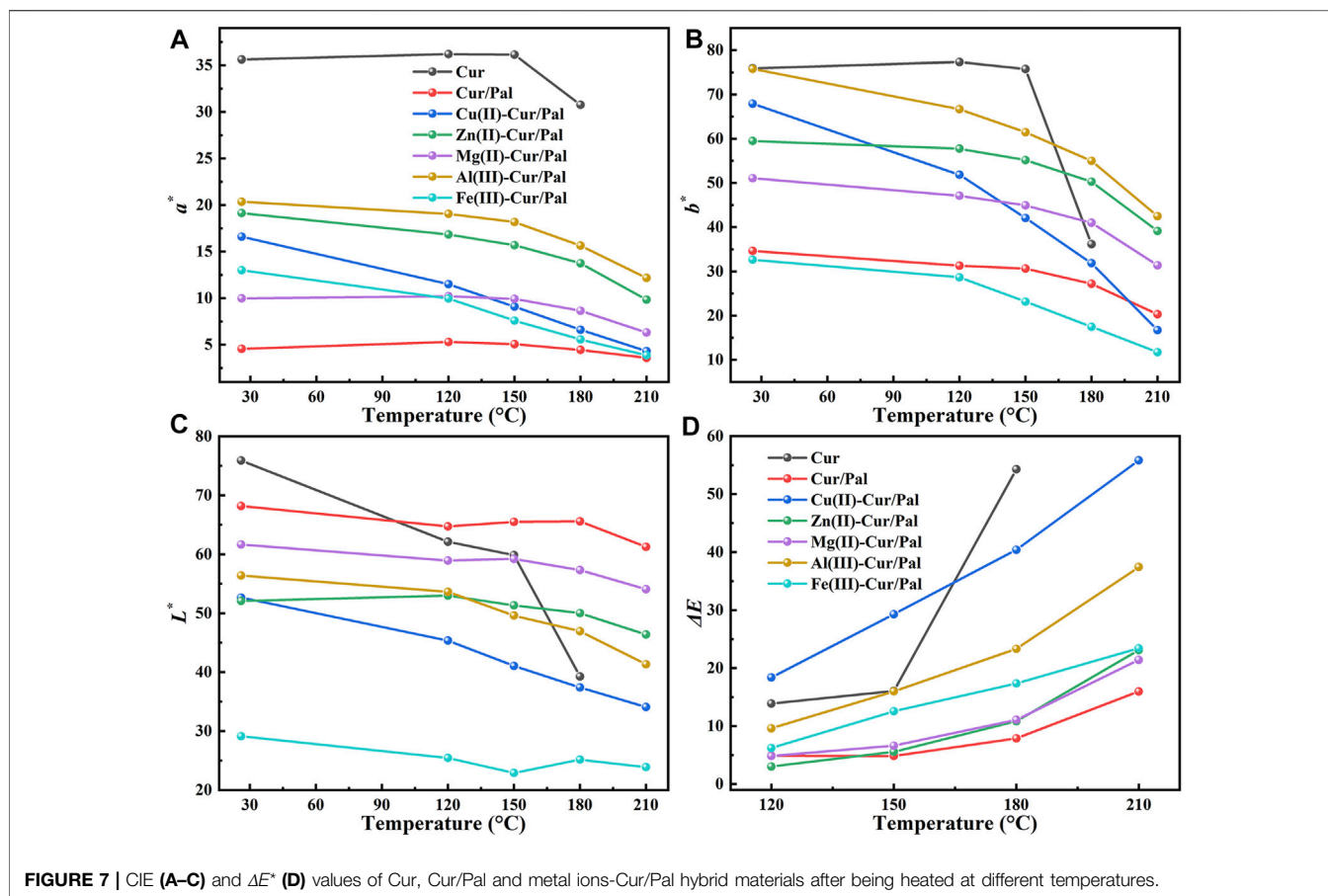## Structural Models of Cur/Pal and Metal Ions-Cur/Pal on DFT Calculation

As shown in **Supplementary Figure S3**, there are two possible structures of Cur, one is ketone structure named as Cur I, and the other is enol structure named as Cur II. The ΔG of Cur II in aqueous solution is 3.97 kcal/mol, which is lower than that of Cur I due to the formation of intramolecular hydrogen bonds in Cur II. Therefore, Cur II is more stable than Cur I. The ESP values showed that the minimum value was at the carbonyl group, indicating that the coordination with metal ions mainly occurred at the carbonyl group.

All the possible structural models of coordination structures of metal ions-Cur are presented in **Supplementary Figure S4**. Among them, M-CurI-1 represented the coordination of metal ions with two carbonyl groups of Cur I, M-CurI-2 referred to the coordination of metal ions with one carbonyl group of Cur I while the other carbonyl group was rotated to one side of the molecule through the σ bond. It was worth noting that M-Cur II-1 was

converted to M-CurI-2 due to the metal coordination with the carbonyl group, breaking the intermolecular hydrogen bond force. Both M-Cur I-3/4 and M-Cur II-2 were considered to coordinate one metal ion with two Cur molecules. As shown in **Supplementary Figure S5**, the intramolecular hydrogen bond was broken after the metal coordinated with the carbonyl group of Cur II, leading to the enol structure being converted into ketone, and the converted carbonyl group was rotated to the other side of the molecule due to influencing factors such as sterichindance. Surprisingly, **Supplementary Figure S6** suggested that the UV spectra of various structures were basically consistent with the experimental values. Therefore, it could be concluded thatthe coordination modes between metal ions and Cur was mainly M-Cur I-2, while that of Al ions was Al(III)-Cur I-1 mode. Furthermore, the possible adsorption of Cur by Pal was analyzed in **Supplementary Figure S7**. It found that carbonyl group of Cur II formed hydrogen bond with complexion water existed in the channels of Pal rather than coordinated with Mg^{2+} at the edges of the octahedral layers, resulting in destroying the intramolecular hydrogen bonds of Cur to form Cur I/Pal mode. In the cases of Al(III)-Cur I-1/Pal and Zn(II)-Cur I-2/Pal, both of them were coordinated with Al^{3+} and Zn^{2+} by Si-OH on Pal surface (**Supplementary Figure S8**). In conclusion, the coordination of metal ions with Cur and Si-OH of Pal as well as the hydrogen bond interaction with complexion water existed in the channels of Pal significantly improved the loading capacity of Pal for Cur.

Thermal Stability of Metal Ions-Cur/Pal

The thermal stability of hybrid materials is of great significance for practical application. The TGA curves of Pal, Cur/Pal and metal ions-Cur/Pal hybrid materials are displayed in **Figure 6**. In the case of Pal (**Figure 6A**), it presented four stages of mass loss, consistent with those previously reported (Zhang et al., 2015b). Briefly, the mass loss before 160°C was attributed to the loss of adsorbed water and loosely bound zeolitic H_2O (6.97% weight loss). The small mass loss at 170°C–300°C, corresponding to the 2.75% weight loss, was associated with the mass loss of residual zeolitic H_2O and the first fraction of structural OH_2. The third step occurring at the range of

FIGURE 7 | CIE **(A–C)** and ΔE^* **(D)** values of Cur, Cur/Pal and metal ions-Cur/Pal hybrid materials after being heated at different temperatures.

FIGURE 8 | Antioxidant activity **(A)** and reducing power **(B)** of Cur/Pal and metal ions-Cur/Pal hybrid materials.

300°C–550°C was assigned to the remove of residual structural OH_2, and the weight loss in this step was about 4.32%. The last 1.01% weight loss occurred at 550°C–800°C, corresponding the degradation of structural OH_2 and hydroxyl groups. The decomposition of Cur began at about 190 °C, ascribing to the dehydroxylation of Cur molecules (**Figure 6B**) (Varaprasad et al., 2020). The total mass loss of pure Cur below 500°C reached 43.59%. The thermal decomposition of the prepared samples was the same as that of Pal, which was

also divided into four steps. However, the mass losses were obviously different after the temperature reached about 285°C by comparison different metal ions-Cur/Pal samples, which was due to the decomposition of different amounts of Cur in samples. Obviously, it suggested the thermal stability of as-prepared metal ions-Cur/Pal samples was higher than that of pure Cur.

The thermal stabilities of as-prepared samples were further estimated by heat treating in an oven at 120°C, 150°C, 180°C, and

210°C for 30 min, respectively. The differences in the CIE and color differences (ΔE^*) values of Cur, Cur/Pal and metal ions-Cur/Pal hybrid materials heated at different temperatures are presented in **Figure 7**. Obviously, the highest L^*, a^* and b^* values was obtained for the pure Cur, demonstrating the vivid color. There was no significant variation in a^* and b^* values after being heated to 150°C, but these values dropped sharply when Cur was heated at 180°C, and the degradation occurred as temperatures continued to rise. The L^* value of Cur decreased sharply with the increase of temperature, indicating a gradual dimming of brightness (**Figures 7A–C**). Although the ΔE^* value of Cur/Pal changed slightly at different temperatures, the a^* and b^* values of Cur/Pal were obviously lower than that of metal ions-Cur/Pal (**Figure 7D**). It might be attributed to the fact that metal ions contributed to enhancing the loading capacity of Cur on Pal, resulting in the initial huge of the samples was significantly superior to Cur/Pal. The above result was consistent with the thermogravimetric data. Furthermore, the prepared samples exhibited a much more limitedchanges in color, L^*, a^*, b^*, and ΔE above 150°C compared with pure Cur (**Supplementary Figure S9**), showing the optimal thermal stabilities.

Antioxidant Activity of Metal Ions-Cur/Pal

It has been established that Cur has excellent antioxidant properties and is a powerful scavenger of various reactive oxygen species due to the presence of the two phenol-OH group, the enol form of the diketone moiety, and the extended conjugated structure (Ak and Gulcin 2008; Shakeri et al., 2019). **Figure 8** demonstrates antioxidant activity and reducing power of Cur/Pal and metal ions-Cur/Pal hybrid materials. It was obvious that the metal ions-Cur/Pal had increased free radical scavenging activity compared with Cur/Pal (**Figure 8A**). The significantly improved antioxidant activity of the metal ions-Cur/Pal complexes might be due to the acquisition of additional superoxide dismutating centers (De Souza and De Giovani, 2004; Shakeri et al., 2019). Among them, Cu(II)-Cur/Pal possessed the highest antioxidant activity, which could be ascribed to the weaker O-H bond exist in the case of Cu(II)-Cur, resulting in easier H-atom loss process in o-methoxy phenolic group (Bagchi et al., 2015). In the rest metal ions-Cur/Pal samples, the existence of stronger O-H bond resulted in the radical scavenging capacity lesser than that of Cu(II)-Cur/Pal (Zhao et al., 2010; Bagchi et al., 2015). Cur with stable electron donor properties could neutralize free radicals by forming stable products, resulting in the termination of the radical chain reactions (Ak and Gulcin 2008). As presented in **Figure 8B**, the result of radical scavenging activity was in line with the reducing power. Of note, ferrous reducing power activities of metal ions-Cur/Pal were also much more effective and powerful reducing ability than the Cur/Pal.

CONCLUSION

In conclusion, the Cur/Pal and metal ions-Cur/Pal complexes with different huge were designed and synthesized based on natural Cur dye and Pal by a simple method, in which natural Pal was served as effective carrier for loading the Cur-metal ions complex. The effect of different metal ions including Cu^{2+}, Zn^{2+}, Mg^{2+}, Al^{3+}, and Fe^{3+} on the huge, environmental stability, antioxidant activity, and fluorescence properties of Cur in the presence of Pal was evaluated. In the case of Cur/Pal, Cur molecule might have formed a complex with H_2O, which was coordinated with Mg^{2+} along the edges of the octahedral layers of Pal. Compared with Cur/Pal composites, the as-prepared composites showed more excellent properties due to the presence of metal ions. The results indicated that the color change and stability enhancement were attributed to the coordination of metal ions with Cur and Si-OH of Pal as well as the hydrogen bond interaction with complexion water existed in the channels of Pal. Therefore, the as-prepared multifunctional composites with different colors and good stability present the potential applications in the relevant fields based on Cur and Pal.

DATA AVAILABILITY STATEMENT

The raw data supporting the conclusion of this article will be made available by the authors, without undue reservation.

AUTHOR CONTRIBUTIONS

AW, BM, and SL designed experiments and analyzed experimental results and wrote the manuscript. PY performed the density functional theory calculation. YK and QW assisted with the experimental work. All authors contributed to the article and agreed to the submitted version.

FUNDING

SUPPLEMENTARY MATERIAL

The Supplementary Material for this article can be found online at: https://www.frontiersin.org/articles/10.3389/fchem.2021.760941/full#supplementary-material.

REFERENCES

Ak, T., and Gulçin, İ. (2008). Antioxidant and Radical Scavenging Properties of Curcumin. *Chem. Biol. Interact.* 174, 27–37. doi:10.1016/j.cbi.2008.05.003

Arab, C., El Kurdi, R., and Patra, D. (2021). Efficient Removal of Congo Red Using Curcumin Conjugated Zinc Oxide Nanoparticles as New Adsorbent Complex. *Chemosphere* 276, 130158. doi:10.1016/j.chemosphere.2021.130158

Bagchi, D., Chaudhuri, S., Sardar, S., Choudhury, S., Polley, N., Lemmens, P., et al. (2015). Modulation of Stability and Functionality of a Phyto-Antioxidant by Weakly Interacting Metal Ions: Curcumin in Aqueous Solution. *RSC Adv.* 5, 102516–102524. doi:10.1039/c5ra21593e

Barik, A., Mishra, B., Kunwar, A., Kadam, R. M., Shen, L., Dutta, S., et al. (2007). Comparative Study of Copper(II)-curcumin Complexes as Superoxide Dismutase Mimics and Free Radical Scavengers. *Eur. J. Med. Chem.* 42, 431–439. doi:10.1016/j.ejmech.2006.11.012

Becke, A. D. (1993). Density-functional Thermochemistry. III. The Role of Exact Exchange. *J. Chem. Phys.* 98, 5648–5652. doi:10.1063/1.464913

Beneduci, A., Corrente, G. A., Marino, T., Aiello, D., Bartella, L., Di Donna, L., et al. (2019). Insight on the Chelation of Aluminum(III) and Iron(III) by Curcumin in Aqueous Solution. *J. Mol. Liquids* 296, 111805. doi:10.1016/j.molliq.2019.111805

Bhopate, D. P., Mahajan, P. G., Garadkar, K. M., Kolekar, G. B., and Patil, S. R. (2015). A Highly Selective and Sensitive Single Click Novel Fluorescent Off-On Sensor for Copper and Sulfide Ions Detection Directly in Aqueous Solution Using Curcumin Nanoparticles. *New J. Chem.* 39, 7086–7096. doi:10.1039/c5nj01228g

Carazo, E., Borrego-Sánchez, A., García-Villén, F., Sánchez-Espejo, R., Viseras, C., Cerezo, P., et al. (2018). Adsorption and Characterization of Palygorskite-Isoniazid Nanohybrids. *Appl. Clay Sci.* 160, 180–185. doi:10.1016/j.clay.2017.12.027

Chen, S., Wu, J., Tang, Q., Xu, C., Huang, Y., Huang, D., et al. (2020). Nano-micelles Based on Hydroxyethyl Starch-Curcumin Conjugates for Improved Stability, Antioxidant and Anticancer Activity of Curcumin. *Carbohydr. Polym.* 228, 115398. doi:10.1016/j.carbpol.2019.115398

Cheng, C., Peng, S., Li, Z., Zou, L., Liu, W., and Liu, C. (2017). Improved Bioavailability of Curcumin in Liposomes Prepared Using a pH-Driven, Organic Solvent-free, Easily Scalable Process. *RSC Adv.* 7, 25978–25986. doi:10.1039/c7ra02861j

De Souza, R. F. V., and De Giovani, W. F. (2004). Antioxidant Properties of Complexes of Flavonoids with Metal Ions. *Redox Rep.* 9, 97–104. doi:10.1179/135100004225003897

Dennington, R., Keith, T., and Millam, J. (2009). *GaussView, Version 5*. Shawnee Mission KS: Semichem Inc.

Doménech-Carbó, A., Valle-Algarra, F. M., Doménech-Carbó, M. T., Domine, M. E., Osete-Cortina, L., and Gimeno-Adelantado, J. V. (2013). Redox Tuning and Species Distribution in Maya Blue-type Materials: a Reassessment. *ACS Appl. Mater. Inter.* 5, 8134–8145. doi:10.1021/am402193u

Frisch, M. J., Trucks, G. W., Schlegel, H. B., Scuseria, G. E., and Fox, D. J. (2009). *Gaussian 09 Revision A.1*, 103. Wallingford, CT: Gaussian Inc., 105636.

Gonçalves, J. L. S., Valandro, S. R., Poli, A. L., and Schmitt, C. C. (2017). Influence of clay Minerals on Curcumin Properties: Stability and Singlet Oxygen Generation. *J. Mol. Struct.* 1143, 1–7. doi:10.1016/j.molstruc.2017.04.073

Goswami, T. K., Gadadhar, S., Gole, B., Karande, A. A., and Chakravarty, A. R. (2013). Photocytotoxicity of Copper(II) Complexes of Curcumin and N-Ferrocenylmethyl-L-Amino Acids. *Eur. J. Med. Chem.* 63, 800–810. doi:10.1016/j.ejmech.2013.03.026

Grimme, S., Antony, J., Ehrlich, S., and Krieg, H. (2010). A Consistent and Accurate ab initio Parametrization of Density Functional Dispersion Correction (DFT-D) for the 94 Elements H-Pu. *J. Chem. Phys.* 132, 154104. doi:10.1063/1.3382344

Grimme, S. (2006). Semiempirical GGA-type Density Functional Constructed with a Long-Range Dispersion Correction. *J. Comput. Chem.* 27, 1787–1799. doi:10.1002/jcc.20495

Gulcin, W., Sat, I. G., Beydemir, S., Elmastas, M., and Kufrevioglu, O. I. (2004). Comparison of Antioxidant Activity of Clove (Eugenia Caryophylata Thunb) Buds and Lavender (Lavandula Stoechas L.). *Food Chem.* 87, 393–400. doi:10.1016/j.foodchem.2003.12.008

Gutiérrez, T. J., Ponce, A. G., and Alvarez, V. A. (2017). Nano-clays from Natural and Modified Montmorillonite with and without Added Blueberry Extract for Active and Intelligent Food Nanopackaging Materials. *Mater. Chem. Phys.* 194, 283–292. doi:10.1016/j.matchemphys.2017.03.052

Howaili, F., Özliseli, E., Küçüktürkmen, B., Razavi, S. M., Sadeghizadeh, M., and Rosenholm, J. M. (2020). Stimuli-Responsive, Plasmonic Nanogel for Dual Delivery of Curcumin and Photothermal Therapy for Cancer Treatment. *Front. Chem.* 8, 602941. doi:10.3389/fchem.2020.602941

Hu, Y., He, C., Jiang, C., Liao, Y., Xiong, H., and Zhao, Q. (2020). Complexation with Whey Protein Fibrils and Chitosan: A Potential Vehicle for Curcumin with Improved Aqueous Dispersion Stability and Enhanced Antioxidant Activity. *Food Hydrocoll.* 104, 105729. doi:10.1016/j.foodhyd.2020.105729

Humphrey, W., Dalke, A., and Schulten, K. (1996). VMD: Visual Molecular Dynamics. *J. Mol. Graph.* 14, 33–38. doi:10.1016/0263-7855(96)00018-5

Jin, T.-r. (2018). Curcumin and Dietary Polyphenol Research: beyond Drug Discovery. *Acta Pharmacol. Sin.* 39, 779–786. doi:10.1038/aps.2017.179

Kumar, A., Hodnett, B. K., Hudson, S., and Davern, P. (2020a). Modification of the Zeta Potential of Montmorillonite to Achieve High Active Pharmaceutical Ingredient Nanoparticle Loading and Stabilization with Optimum Dissolution Properties. *Colloids Surf. B Biointerfaces* 193, 111120. doi:10.1016/j.colsurfb.2020.111120

Kumar, R., Uppal, S., Kaur, K., and Mehta, S. K. (2020b). Curcumin Nanoemulsion as a Biocompatible Medium to Study the Metal Ion Imbalance in a Biological System. *J. Mol. Liquids* 314, 113611. doi:10.1016/j.molliq.2020.113611

Li, S., Ding, J., Mu, B., Wang, X., Kang, Y., and Wang, A. (2019a). Acid/base Reversible Allochroic Anthocyanin/palygorskite Hybrid Pigments: Preparation, Stability and Potential Applications. *Dyes Pigm.* 171, 107738. doi:10.1016/j.dyepig.2019.107738

Li, S., Mu, B., Wang, X., Kang, Y., and Wang, A. (2019b). A Comparative Study on Color Stability of Anthocyanin Hybrid Pigments Derived from 1D and 2D Clay Minerals. *Materials* 12 (20), 3287. doi:10.3390/ma12203287

Li, S., Mu, B., Wang, X., Kang, Y., and Wang, A. (2020a). Fabrication of Eco-Friendly Betanin Hybrid Materials Based on Palygorskite and Halloysite. *Materials (Basel)* 13, 4649. doi:10.3390/ma13204649

Li, Z., Shi, M., Li, N., and Xu, R. (2020b). Application of Functional Biocompatible Nanomaterials to Improve Curcumin Bioavailability. *Front. Chem.* 8, 589957. doi:10.3389/fchem.2020.589957

Li, X. (2012). Improved Pyrogallol Autoxidation Method: a Reliable and Cheap Superoxide-Scavenging Assay Suitable for All Antioxidants. *J. Agric. Food Chem.* 60, 6418–6424. doi:10.1021/jf204970r

Liao, Y., Yao, Y., Yu, Y., and Zeng, Y. (2018). Enhanced Antibacterial Activity of Curcumin by Combination with Metal Ions. *Colloid Interf. Sci. Commun.* 25, 1–6. doi:10.1016/j.colcom.2018.04.009

Lin, X., Shi, Y., Yu, S., Li, S., Li, W., Li, M., et al. (2020). Preparation of Poloxamer188-B-PCL and Study on In Vitro Radioprotection Activity of Curcumin-Loaded Nanoparticles. *Front. Chem.* 8, 212. doi:10.3389/fchem.2020.00212

Lu, T., and Chen, F. (2012). Multiwfn: a Multifunctional Wavefunction Analyzer. *J. Comput. Chem.* 33, 580–592. doi:10.1002/jcc.22885

Lu, Y., Dong, W., Wang, W., Wang, Q., Hui, A., and Wang, A. (2019). A Comparative Study of Different Natural Palygorskite Clays for Fabricating Cost-Efficient and Eco-Friendly Iron Red Composite Pigments. *Appl. Clay Sci.* 167, 50–59. doi:10.1016/j.clay.2018.10.008

Ma, Q., Du, L., and Wang, L. (2017). Tara Gum/polyvinyl Alcohol-Based Colorimetric NH3 Indicator Films Incorporating Curcumin for Intelligent Packaging. *Sensors Actuators B: Chem.* 244, 759–766. doi:10.1016/j.snb.2017.01.035

Madusanka, N., de Silva, K. M. N., and Amaratunga, G. (2015). A Curcumin Activated Carboxymethyl Cellulose-Montmorillonite clay Nanocomposite Having Enhanced Curcumin Release in Aqueous media. *Carbohydr. Polym.* 134, 695–699. doi:10.1016/j.carbpol.2015.08.030

Mandal, B., Rameshbabu, A. P., Soni, S. R., Ghosh, A., Dhara, S., and Pal, S. (2017). *In Situ* Silver Nanowire Deposited Cross-Linked Carboxymethyl Cellulose: A Potential Transdermal Anticancer Drug Carrier. *ACS Appl. Mater. Inter.* 9, 36583–36595. doi:10.1021/acsami.7b10716

Marenich, A. V., Cramer, C. J., and Truhlar, D. G. (2009). Universal Solvation Model Based on Solute Electron Density and on a Continuum Model of the Solvent Defined by the Bulk Dielectric Constant and Atomic Surface Tensions. *J. Phys. Chem. B* 113, 6378–6396. doi:10.1021/jp810292n

Mary, C. P. V., Vijayakumar, S., and Shankar, R. (2018). Metal Chelating Ability and Antioxidant Properties of Curcumin-Metal Complexes - A DFT Approach. *J. Mol. Graph. Model.* 79, 1–14. doi:10.1016/j.jmgm.2017.10.022

Miao, W., Gan, S., Li, X., and Lv, Y. (2020). A Triply Synergistic Method for Palygorskite Activation to Effectively Impregnate Phase Change Materials (PCMs) for thermal Energy Storage. *Appl. Clay Sci.* 189, 105530. doi:10.1016/j.clay.2020.105530

Mohammadian, M., Salami, M., Momen, S., Alavi, F., Emam-Djomeh, Z., and Moosavi-Movahedi, A. A. (2019). Enhancing the Aqueous Solubility of Curcumin at Acidic Condition through the Complexation with Whey Protein Nanofibrils. *Food Hydrocoll.* 87, 902–914. doi:10.1016/j.foodhyd.2018.09.001

Moradi, G., Zinadini, S., Rajabi, L., and Ashraf Derakhshan, A. (2020). Removal of Heavy Metal Ions Using a New High Performance Nanofiltration Membrane Modified with Curcumin Boehmite Nanoparticles. *Chem. Eng. J.* 390, 124546. doi:10.1016/j.cej.2020.124546

Picciano, A. L., and Vaden, T. D. (2013). Complexation between Cu(II) and Curcumin in the Presence of Two Different Segments of Amyloid β. *Biophys. Chem.* 184, 62–67. doi:10.1016/j.bpc.2013.09.004

Pourreza, N., Lotfizadeh, N., and Golmohammadi, H. (2018). Colorimetric Sensing of Oxalate Based on its Inhibitory Effect on the Reaction of Fe (III) with Curcumin Nanoparticles. *Spectrochim. Acta A: Mol. Biomol. Spectrosc.* 192, 251–256. doi:10.1016/j.saa.2017.11.003

Priyadarsini, K. I., Maity, D. K., Naik, G. H., Kumar, M. S., Unnikrishnan, M. K., Satav, J. G., et al. (2003). Role of Phenolic O-H and Methylene Hydrogen on the Free Radical Reactions and Antioxidant Activity of Curcumin. *Free Radic. Biol. Med.* 35, 475–484. doi:10.1016/s0891-5849(03)00325-3

Rao, K. M., Kumar, A., Suneetha, M., and Han, S. S. (2018). pH and Near-Infrared Active; Chitosan-Coated Halloysite Nanotubes Loaded with Curcumin-Au Hybrid Nanoparticles for Cancer Drug Delivery. *Int. J. Biol. Macromol.* 112, 119–125. doi:10.1016/j.ijbiomac.2018.01.163

Refat, M. S. (2013). Synthesis and Characterization of Ligational Behavior of Curcumin Drug towards Some Transition Metal Ions: Chelation Effect on Their thermal Stability and Biological Activity. *Spectrochim. Acta Part A: Mol. Biomol. Spectrosc.* 105, 326–337. doi:10.1016/j.saa.2012.12.041

Schwabe, T., and Grimme, S. (2007). Double-hybrid Density Functionals with Long-Range Dispersion Corrections: Higher Accuracy and Extended Applicability. *Phys. Chem. Chem. Phys.* 9, 3397–3406. doi:10.1039/b704725h

Shakeri, A., Panahi, Y., Johnston, T. P., and Sahebkar, A. (2019). Biological Properties of Metal Complexes of Curcumin. *Biofactors* 45 (3), 304–317. doi:10.1002/biof.1504

Silva, G. T. M., Silva, C. P., Gehlen, M. H., Oake, J., Bohne, C., and Quina, F. H. (2018). Organic/inorganic Hybrid Pigments from Flavylium Cations and Palygorskite. *Appl. Clay Sci.* 162, 478–486. doi:10.1016/j.clay.2018.07.002

Song, Y.-M., Xu, J.-P., Ding, L., Hou, Q., Liu, J.-W., and Zhu, Z.-L. (2009). Syntheses, Characterization and Biological Activities of Rare Earth Metal Complexes with Curcumin and 1,10-Phenanthroline-5,6-Dione. *J. Inorg. Biochem.* 103, 396–400. doi:10.1016/j.jinorgbio.2008.12.001

Van Olphen, H. (1966). Maya Blue: A Clay-Organic Pigment?. *Science* 154, 645–646. doi:10.1126/science.154.3749.645

Varaprasad, K., López, M., Núñez, D., Jayaramudu, T., Sadiku, E. R., Karthikeyan, C., et al. (2020). Antibiotic Copper Oxide-Curcumin Nanomaterials for Antibacterial Applications. *J. Mol. Liquids* 300, 112353. doi:10.1016/j.molliq.2019.112353

Wang, X., Mu, B., An, X., and Wang, A. (2018). Insights into the Relationship between the Color and Photocatalytic Property of attapulgite/CdS Nanocomposites. *Appl. Surf. Sci.* 439, 202–212. doi:10.1016/j.apsusc.2018.01.054

Wang, Y., Ying, T., Li, J., Xu, Y., Wang, R., Ke, Q., et al. (2020). Hierarchical Micro/nanofibrous Scaffolds Incorporated with Curcumin and Zinc Ion Eutectic Metal Organic Frameworks for Enhanced Diabetic Wound Healing via Anti-oxidant and Anti-inflammatory Activities. *Chem. Eng. J.* 402, 126273. doi:10.1016/j.cej.2020.126273

Wei, Y., Nie, Y., Han, Z., Huang, H., Liao, X., Wang, X., et al. (2021). Au@polydopamine Nanoparticles/tocilizumab Composite as Efficient Scavengers of Oxygen Free Radicals for Improving the Treatment of Rheumatoid Arthritis. *Mater. Sci. Eng. C* 118, 111434. doi:10.1016/j.msec.2020.111434

Xu, J., Wang, W., Gao, J., and Wang, A. (2017). Fabrication of Stable glycine/palygorskite Nanohybrid via High-Pressure Homogenization as High-Efficient Adsorbent for Cs(I) and Methyl Violet. *J. Taiwan Inst. Chem. Eng.* 80, 997–1005. doi:10.1016/j.jtice.2017.09.003

Yuan, Y., Ma, M., Zhang, S., Liu, C., Chen, P., Li, H., et al. (2021). Effect of Sophorolipid on the Curcumin-Loaded Ternary Composite Nanoparticles Self-Assembled from Zein and Chondroitin Sulfate. *Food Hydrocoll.* 113, 106493. doi:10.1016/j.foodhyd.2020.106493

Zhang, Y., Wang, W., Zhang, J., Liu, P., and Wang, A. (2015a). A Comparative Study about Adsorption of Natural Palygorskite for Methylene Blue. *Chem. Eng. J.* 262, 390–398. doi:10.1016/j.cej.2014.10.009

Zhang, Y., Zhang, J., and Wang, A. (2015b). Facile Preparation of Stable Palygorskite/methyl violet@SiO2 "Maya Violet" Pigment. *J. Colloid Interf. Sci.* 457, 254–263. doi:10.1016/j.jcis.2015.07.030

Zhang, W., Chen, C., Shi, H., Yang, M., Liu, Y., Ji, P., et al. (2016). Curcumin Is a Biologically Active Copper Chelator with Antitumor Activity. *Phytomedicine* 23, 1–8. doi:10.1016/j.phymed.2015.11.005

Zhao, Y., and Truhlar, D. G. (2008). The M06 Suite of Density Functionals for Main Group Thermochemistry, Thermochemical Kinetics, Noncovalent Interactions, Excited States, and Transition Elements: Two New Functionals and Systematic Testing of Four M06-Class Functionals and 12 Other Functionals. *Theor. Chem. Account.* 120, 215–241. doi:10.1007/s00214-007-0310-x

Zhao, X.-Z., Jiang, T., Wang, L., Yang, H., Zhang, S., and Zhou, P. (2010). Interaction of Curcumin with Zn(II) and Cu(II) Ions Based on experiment and Theoretical Calculation. *J. Mol. Struct.* 984, 316–325. doi:10.1016/j.molstruc.2010.09.049

Zhou, Y., and Tang, R.-C. (2016). Modification of Curcumin with a Reactive UV Absorber and its Dyeing and Functional Properties for Silk. *Dyes Pigm.* 134, 203–211. doi:10.1016/j.dyepig.2016.07.016